**Supplementary Information**

# [100] directed Cu-doped h-CoO Nanorods: Elucidation of Growth Mechanism and Application to Lithium-Ion Batteries

*Ki Min Nam*[†], *Young Cheol Choi*[‡], *Sung Chul Jung*[€], *Yong-Il Kim*[¶], *Mi Ru Jo*[§], *Se Ho Park*[†], *Yong-Mook Kang*[§,*], *Young-Kyu Han*[€,*] *and Joon T. Park*[†,*]

Department of Chemistry, Korea Advanced Institute of Science and Technology (KAIST), Daejeon, 305-701, Korea, Corporate R&D, LG Chem., Ltd. Research Park, Daejeon, 305-380, Korea, Division of Advanced Materials Engineering, Kongju National University, 275 Budae-dong, Cheonan, Chungnam, Korea, Korea Research Institute of Standards and Science (KRISS), Daejeon, 305-340, Korea, Division of Materials Science, Korea Basic Science Institute (KBSI), Daejeon, 305-333, Korea

***RECEIVED DATE (automatically inserted by publisher)****; E-mail: joontpark@kaist.ac.kr; ykhan@kbsi.re.kr; dake1234@kongju.ac.kr*

† Department of Chemistry, KAIST

‡ LG Chem. Ltd. Research Park

§ Kongju National University

¶ KRISS

€ Division of Materials Science, KBSI

## Experimental Section

### General Methods

The synthesis of h-CoO was carried out using standard Schlenk techniques under an argon atmosphere. $Co(acac)_3$ (99.99 +%, Sigma-Aldrich), $Cu(acac)_2$ (99.99 +%, Sigma-Aldrich) and benzylamine (99 %, Sigma-Aldrich) were used without further purification.

**Computational details.** The plane-wave pseudopotential calculations were performed using the Vienna Ab Initio Simulation Package (VASP)[1] with the projector augmented wave (PAW) construction for the pseudopotential.[2] The exchange-correlation was described within the generalized gradient approximation (GGA) with the on-site Coulomb interactions described in terms of a Hubbard U,[3] where we used the Perdew–Burke–Ernzerhof (PBE) functional[4] and the Hubbard U of 5.3 eV for the Co 3*d* orbital. The plane-wave cutoff was set to 400 eV throughout the calculations. For the dense mesh of the Brillouin-zone integration, at least 24 irreducible k-points per 1×1 surface unit cell were used. The lattice constants and the atomic coordinates of the wurtzite-type of bulk CoO were fully relaxed, and the slab lattice constants were set equal to the bulk value in a direction parallel to the surface. Slabs with 10, 18, 13, and 19 atomic layers containing 20, 36, 52, and 38 atoms were used for the (001), (100), (110), and (101) surfaces, respectively. The atomic coordinates were relaxed until the forces acting on the atoms did not exceed 0.02 eV/Å. Figure S7 presents side views for the optimized structures of the pure h-CoO and Cu-doped h-CoO slab models. To prevent the interaction between slabs through the vacuum region, the neighboring slabs were separated by more than 10 Å and the dipole correction[5] was employed. The surface energies were obtained by computing the total energy differences between a unit cell of slab model and the same amount of bulk material, in which the bulk CoO with 1/36 Cu-doping (~3 % uniform doping) was used as the reference bulk material for the surface energy calculations of Cu-doped h-CoO system.

### References

(1) (a) G. Kresse, J. Hafner, *Phys. Rev. B* **1993**, *47*, R558. (b) G. Kresse, J. Furtmüller, *Phys. Rev. B* **1996**, *54*, 11169.

(2) (a) P. E. Blöchl, *Phys. Rev. B* **1994**, *50*, 17953. (b) G. Kresse, J. Joubert, *Phys. Rev. B* **1999**, *59*, 1758.

(3) (a) V. I. Anisimov, F. Aryasetiawan, A. I. Liechtenstein, *J. Phys.: Condens. Matter* **1997**, *9*, 767. (b) A. Rohrbach, J. Hafner, G. Kresse, *J. Phys.: Condens. Matter* **2003**, *15*, 979.

(4) J. P. Perdew, K. Burke, M. Ernzerhof, *Phys. Rev. Lett*. **1996**, *77*, 3865.

(5) J. Neugebauer, M. Scheffler, *Phys. Rev. B* **1992**, *46*, 16067.

## Formation energy calculation

We have calculated the formation energies for the Cu doping into CoO bulk to determine preferable sites for Cu. The formation energy Ω is given by

$\Omega = E_{tot} - n_{Co}\mu_{Co} - n_O\mu_O - n_{Cu}\mu_{Cu}$,

where $E_{tot}$ is the total energy of the doped CoO bulk, $n$'s are the numbers of atoms in the unit cell, and $\mu$'s are the corresponding atomic chemical potentials [1]. With the use of a constraint $\mu_{Co} + \mu_O = \mu_{CoO(bulk)}$, the above equation is written as

$\Omega = E'_{tot} - (n_{Co} - n_O)\Delta\mu/2 - n_{Cu}(\mu_{Cu} - \mu_{Cu(bulk)})$

where $E'_{tot} = E_{tot} - (n_{Co} + n_O)\mu_{CoO(bulk)}/2 - (n_{Co} - n_O)(\mu_{Co(bulk)} - \mu_{O(gas)})/2 - n_{Cu}\mu_{Cu(bulk)}$,

and $\Delta\mu = (\mu_{Co} - \mu_O) - (\mu_{Co(bulk)} - \mu_{O(gas)})$ [1].

The chemical potential difference $\Delta\mu$ varies over a range limited by the inequalities $\mu_{Co} \le \mu_{Co(bulk)}$ and $\mu_O \le \mu_{O(gas)}$. The allowed range of $\Delta\mu$ is given as $-\Delta H \le \Delta\mu \le \Delta H$ by using the heat of formation of CoO, defined as $\Delta H = \mu_{Co(bulk)} + \mu_{O(gas)} - \mu_{CoO(bulk)}$. In the present system, $\Delta H$ is calculated to be 3.375 eV. We consider three doping models, i.e., the substitution of Co by Cu ($Cu_{Co}$), the substitution of O by Cu ($Cu_O$), and the occupation of interstitial sites by Cu ($Cu_i$), and calculate the relative formation energy $\Delta\Omega = \Omega + \mu_{Cu} - \mu_{Cu(bulk)}$ as a function of $\Delta\mu$ [2] for the doping of a single Cu atom into CoO bulk with 36 Co and 36 O atoms (see the Figure below). It is clear that, of the three models, the substitution of Co by Cu is favored over accessible chemical potential range, regardless of whether it is the Co-rich or O-rich conditions ($\Delta\mu > 0$ or $\Delta\mu < 0$, respectively).

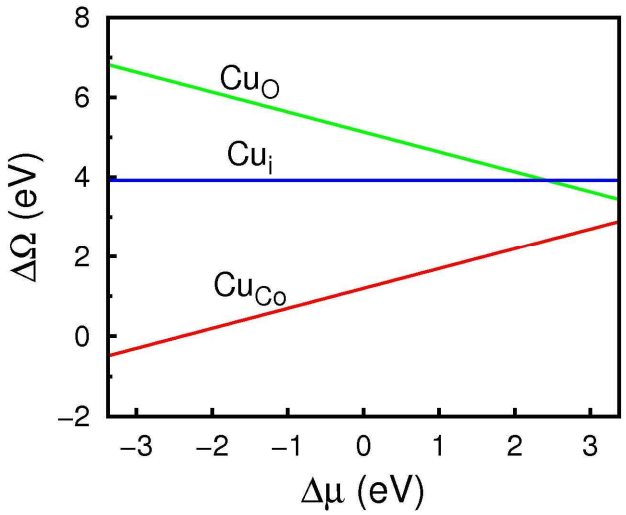


[1] J. E. Northrup, S. B. Zhang, *Phys. Rev. B* **1993**, *47*, 6791.

[2] N. Ghaderi, M. Peressi, N. Binggeli, H. Akbarzadeh, *Phys. Rev. B* **2010**, *81*, 155311.

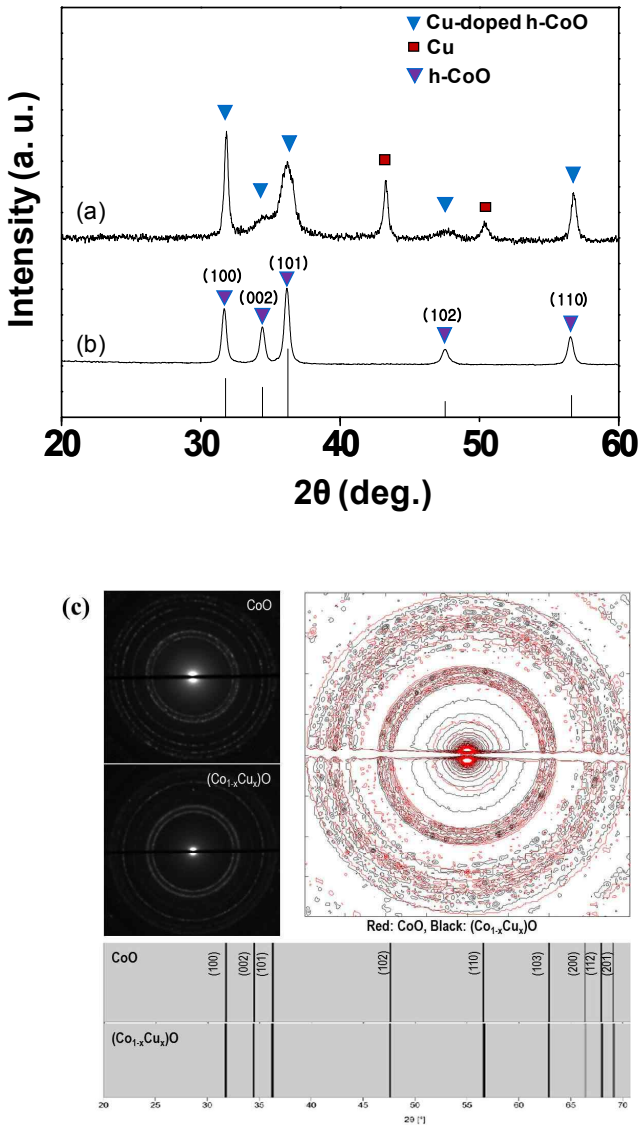


***Figure S1.*** XRD patterns of (a) Cu-doped h-CoO nanorods (the Cu peaks originate from the Cu nanoparticle contaminant) (b) h-CoO nanocrystal. (c) selected area electron diffraction (SAED) patterns of h-CoO and Cu-doped h-CoO nanorods. The overlapped ED pattern shows that there is small but distinct difference from the ED patterns between h-CoO and Cu-doped h-CoO. The red and black colors represent h-CoO and Cu-doped h-CoO, respectively.The diameters of Debye-rings observed from Cu doped h-CoO will be more toward the ring center than those of that of h-CoO because the effective ion radius of $Cu^{2+}$ (0.57 Å) is small comparing with $Co^{2+}$ (0.58 Å). This is the same meaning that the peaks in the X-ray diffraction of Cu-doped h-CoO shift to toward the lower angle than that of h-CoO. The peak shifts toward to lower angle result in the change of lattice parametersof Cu-doped h-CoO.

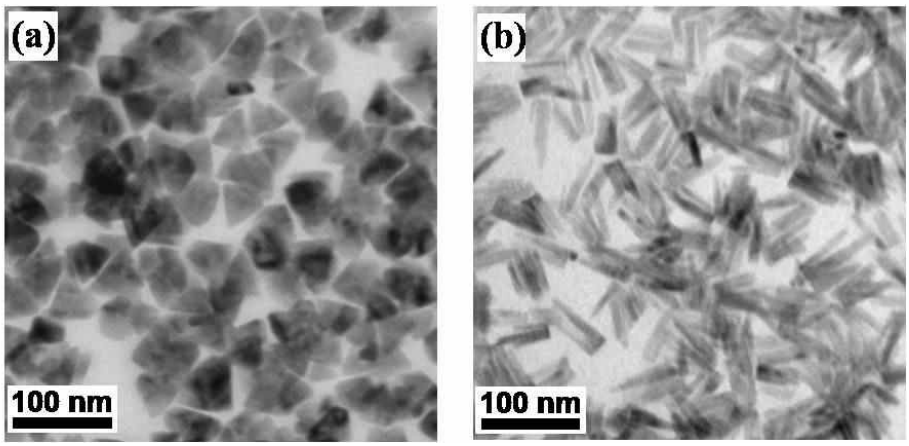


***Figure S2.*** TEM micrographs of (a) h-CoO nanocrystals with an average side edge length of 40 ± 6.4 nm and a basal edge length of 20 ± 5.0 nm, and (b) h-CoO nanorods with an average width of 7 ± 0.9 nm and a length of 65 ± 9.8 nm.

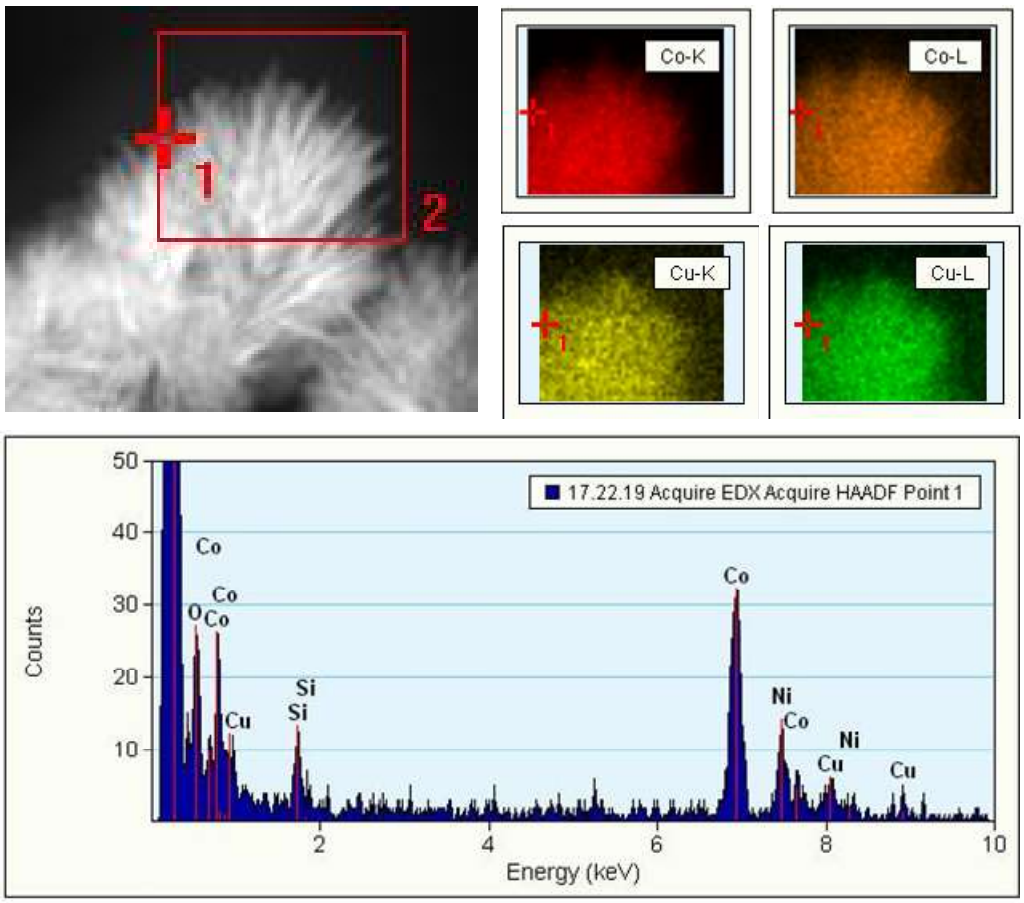


***Figure S3.*** Energy dispersive X-ray spectroscopy (EDX) recorded from a nanorod shows presence of minor copper besides majority of Co and O (Ni and Si signals come from nickel grid and the substrate).

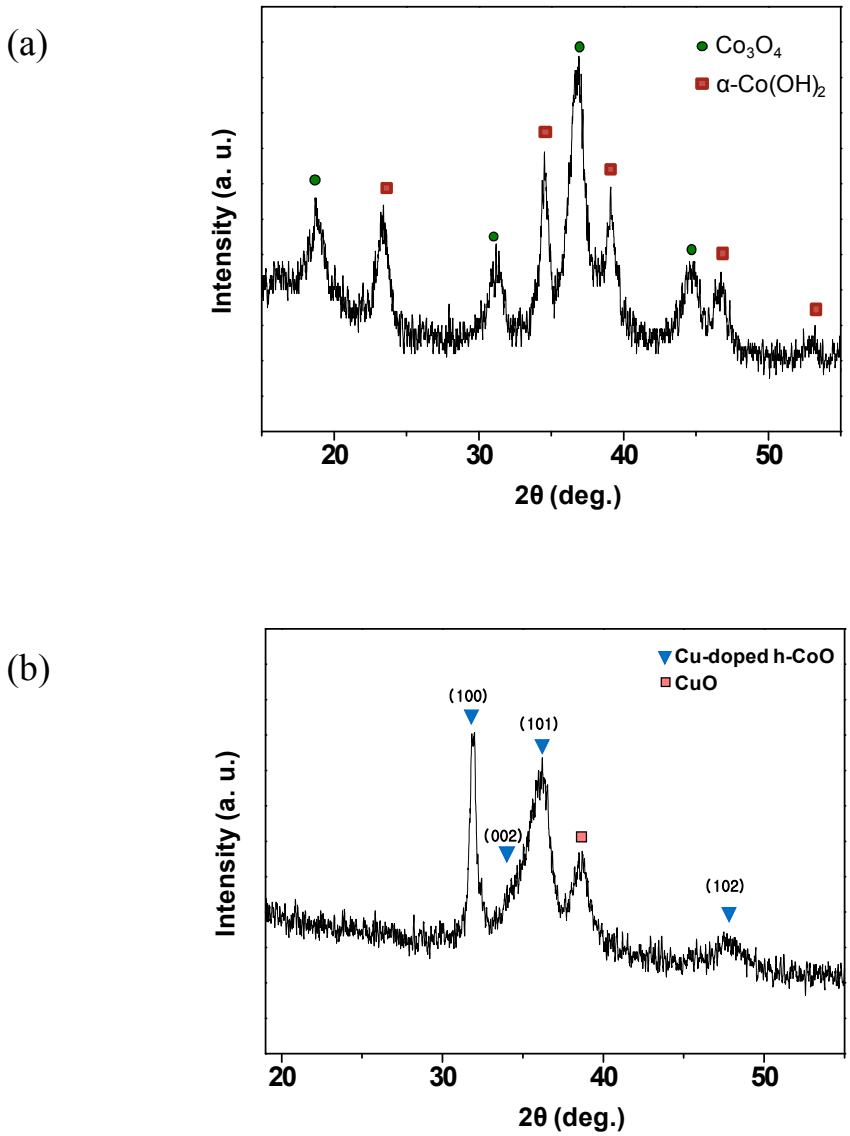


***Figure S4.*** XRD patterns of (a) spinel $Co_3O_4$ and α-$Co(OH)_2$ obtained by water addition to the pure h-CoO nanocrystals, and (b) Cu-doped h-CoO and CuO obtained by water addition to the Cu-doped h-CoO and Cu, respectively.

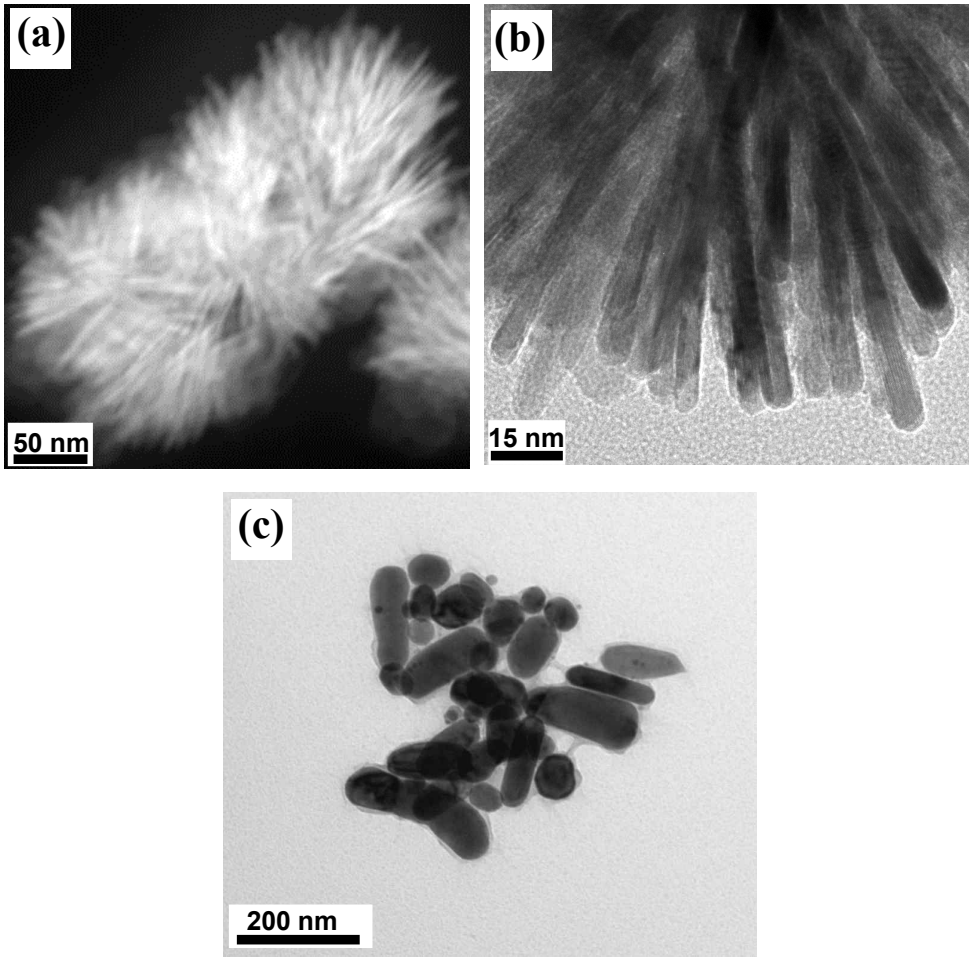


***Figure S5.*** TEM micrographs of Cu-doped h-CoO nanorods and Cu nanoparticles: (a) dark-field TEM image, (b) bright-field TEM image of Cu-doped h-CoO nanorods, and (c) TEM image of Cu nanoparticles

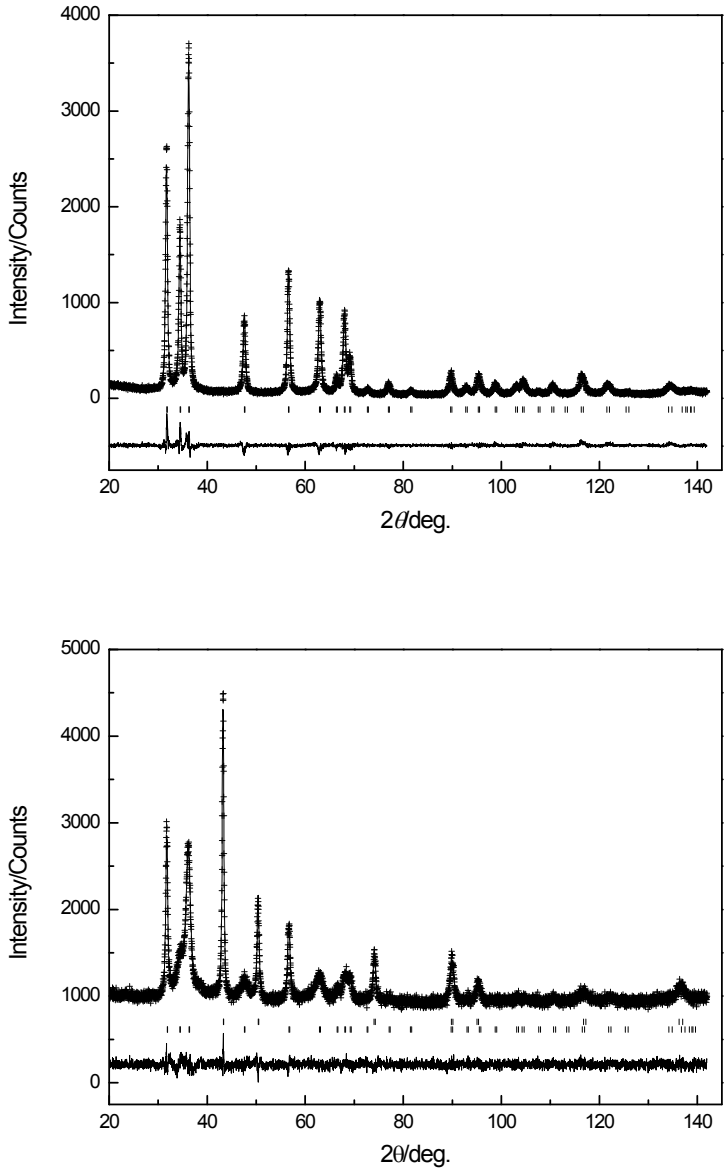


***Figure S6.*** X-ray Rietveld analyses of (a) h-CoO and (b) Cu-doped h-CoO nanorods. Plus signs (+) represent the observed intensities; the solid line is calculated ones. A difference plot (obs. – cal.) is shown beneath. Tick marks above the difference data indicate the reflection position. In h-CoO nanorod, the marks above the difference data indicate the reflection position for h-CoO phase, and in Cu-doped h-CoO nanorod, the upper and lower tick marks correspond to Cu and Cu-doped h-CoO ($Co_{1-x}Cu_xO$) phases. The lattice parameters are described in Table Sl.

***Table S1.*** Refined structural parameters for h-CoO and Cu-doped h-CoO nanorods obtained from Rietveld analysis using X-ray powder diffraction data at room temperature. The symbol, *g*, is the occupation factor. The numbers in parentheses are the estimated standard deviations of the last significant figure.

| Sample | Phase | Lattice parameters (Å) | Weight fraction (%) | Atom | *x/a* | *y/b* | *z/c* | *g* |
|---|---|---|---|---|---|---|---|---|
| (a) h-CoO | CoO | $a(=b) = 3.25063(5)$<br>$c = 5.19875(2)$ | 100 | Co<br>O | 1/3<br>1/3 | 2/3<br>2/3 | 0.0<br>0.384(1) | 1.0<br>1.0 |
| (b) Cu-doped h-CoO | $(Co_{1-x}Cu_x)O$ | $a(=b) = 3.24423(3)$<br>$c = 5.20290(3)$ | 75.6 (2) | Co<br>Cu<br>O | 1/3<br>1/3<br>1/3 | 2/3<br>2/3<br>2/3 | 0.0<br>0.0<br>0.356(3) | 0.97(2)[a]<br>0.03(2)<br>1.0 |
| | Cu | $a(=b=c) = 3.61750(5)$ | 24.4(2) | Cu | 0.0 | 0.0 | 0.0 | 1.0 |

a) Constraint on occupancy: $g(\mathrm{Co}) + g(\mathrm{Cu}) = 1.0$

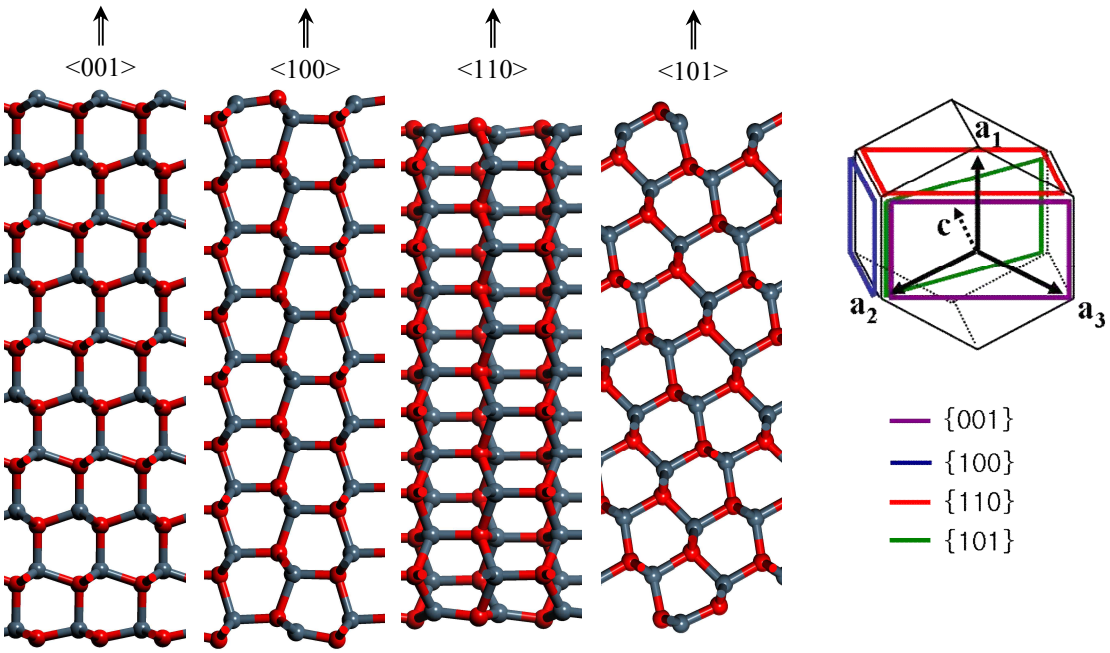


(a) h-CoO

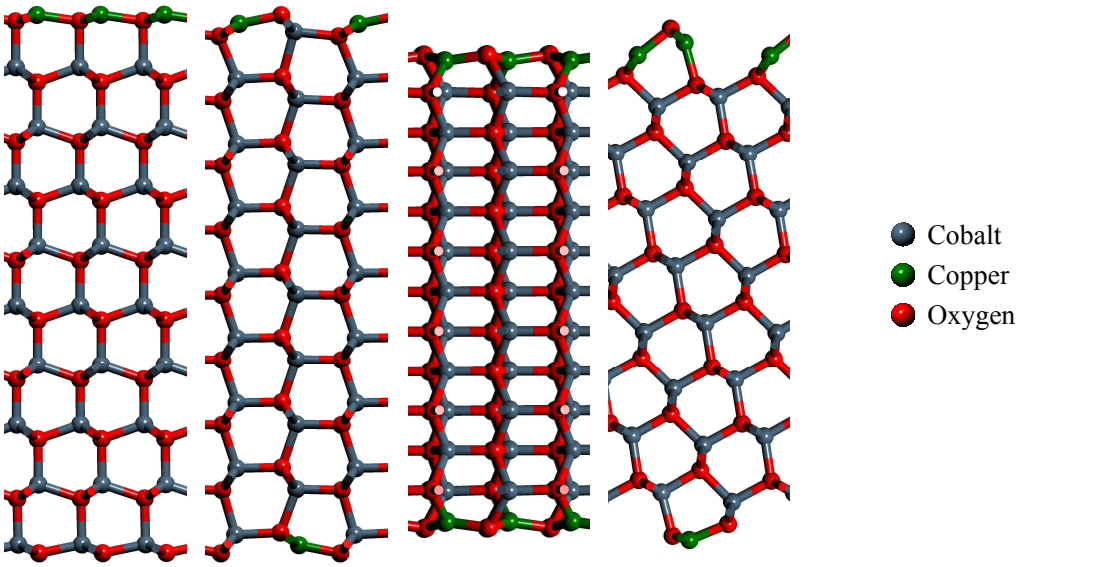


(b) Cu-doped h-CoO

***Figure S7.*** Side views for the optimized structures of the pure h-CoO and Cu-doped h-CoO slab models.

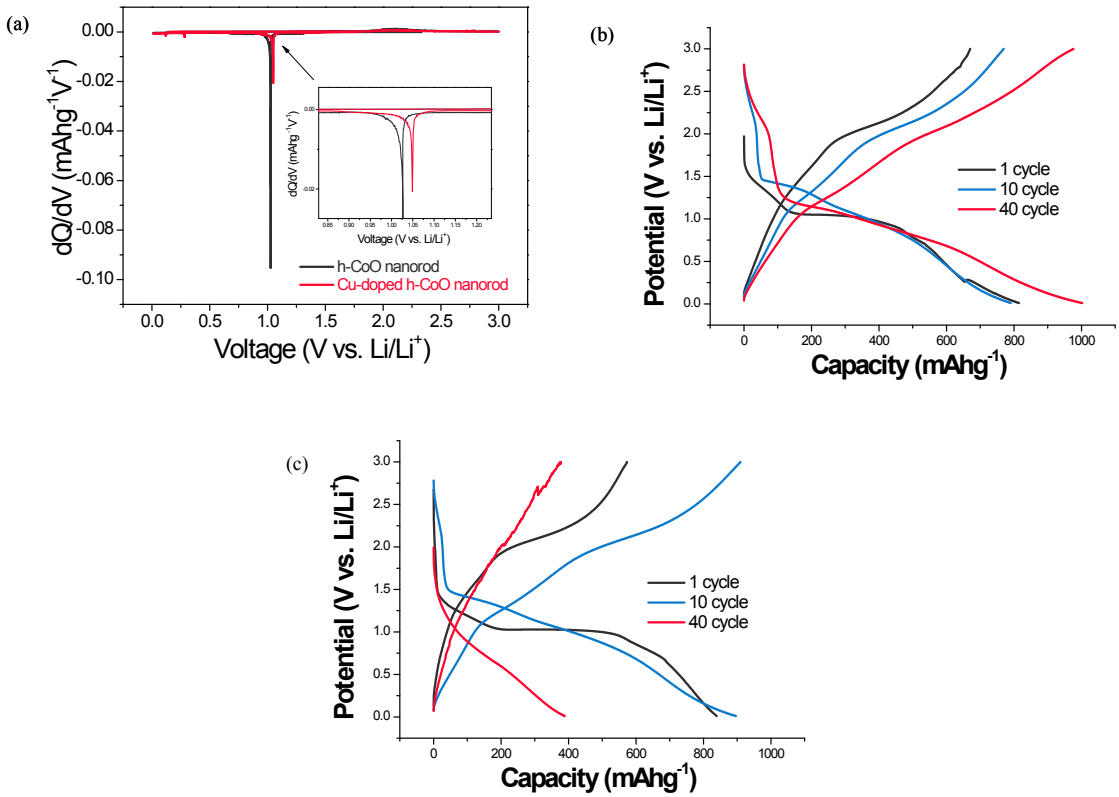


***Figure S8.*** (a) The derivatives dQ/dV plots for the h-CoO nanorod and Cu-doped h-CoO nanorod. Charge-discharge durves of (b) Cu-doped h-CoO nanorods and (c) h-CoO nanorods.